Constraining Mercury Sources Along an Estuarine-to-Marine Sediment Gradient using Mercury and Carbon Stable Isotopes

Alina Kleindienst[1]†*, Alyssa Azaroff[1,2]†, Emmanuel Tessier[1], Alkuin Maximilian Koenig[3], Claudia Marchan Moreno[1], Zoyne Pedrero Zayas[1], David Amouroux[1], Mathilde Monperrus[1]

[1]Université de Pau et des Pays de l'Adour, CNRS, Institut des Sciences Analytiques et de Physico-Chimie pour l'Environnement et les Matériaux (IPREM), Pau, Anglet, France

[2]Department of Environmental Science, Stockholm University, Stockholm, Sweden

[3]Institute of Coastal Systems–Analysis and Modeling, Helmholtz-Zentrum Hereon, Max-Planck-Str. 1, 21502 Geesthacht, Germany

*E-mail: a.kleindienst@univ-pau.fr, david.amouroux@univ-pau.fr

†Alina Kleindienst and Alyssa Azaroff have equally contributed to this work

Abstract

The coastal ocean receives more mercury from riverine input (land-derived Hg) than from direct atmospheric deposition. Land-derived Hg is primarily particle-bound and buried in coastal sediment, where it may undergo methylation. However, its contribution to coastal sediment Hg loads remains poorly constrained.

Here, we investigate Hg sources along an estuarine-to-marine gradient in the Bay of Biscay (Atlantic Ocean) combining Hg and carbon (C) stable isotopic composition in sediments. We find a significant ($p<0.05$) difference in δ^{202}Hg and δ^{13}C between estuarine (δ^{202}Hg -0.83 ± 0.15‰, δ^{13}C -27.3 ± 0.50‰) and marine (δ^{202}Hg -0.54 ± 0.16‰, δ^{13}C -25.2 ± 0.80‰) sediments, and a significant correlation ($p<0.05$) between δ^{13}C and δ^{202}Hg. While in-situ processes had a negligible impact on Hg isotopic composition, the observed trends could be explained by the mixing of land-derived Hg (e.g. vegetational uptake, anthropogenic) and direct atmospheric deposition to the marine environment.

Applying a binary-mixing model with regional endmembers to δ^{13}C and δ^{202} signatures reveals a near 1:1 relationship between land-derived Hg and terrestrial C along our estuarine-to-marine gradient. This relationship, if confirmed for other regions, suggests that joint observations of C stable isotopes and Hg concentrations could directly constrain the transfer of land-derived Hg into coastal sediments.

Keywords (5-8):

Mercury, organic carbon, land-ocean continuum, sediments, stable isotopes, sources

Synopsis Statement:

We show that Hg and C isotopes are jointly diluted over an estuarine-to-marine gradient which suggests that C may be used to trace land-derived Hg inputs and fates in coastal marine sediments.

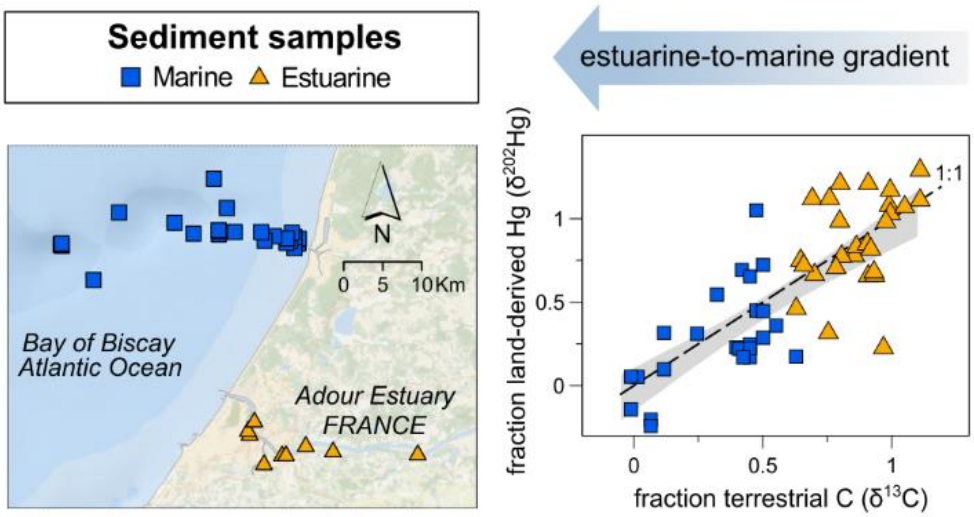

42

43

44

1. Introduction

Estuarine and coastal zones are highly dynamic transition areas between land and sea, receiving continuous riverine input of nutrients, suspended particulate matter, and trace metals including mercury (Hg). The majority of riverine Hg is associated with particulate organic carbon [1,2] and buried in sediments trough particle settling [3,4]. In sediments, Hg may undergo microbial methylation to form methylated Hg (MeHg) [5,6], a potent neurotoxin, which magnifies along the trophic chain resulting in high exposure levels for fish consuming populations [7–9].

For the global coastal ocean, riverine inputsof Hg exceed atmospheric deposition [2]. While reduction of riverine inorganic Hg (Hg(II)) and its evasion to the atmosphere may partially offset the input of terrestrial Hg to the coastal ocean [10], it has been estimated to be of minor importance [2,11,12], likely due to the importance of transient flood events in particle export [2,13].

However, these estimates are highly uncertain, as Earth system models lack adequate representation of estuarine and coastal processes [2], and observational data covering the estuarine-to-marine continuum remain scarce [14–17]. In light of the projected increase in river flood events with climate change, which will likely elevate the Hg burden to coastal zones, and the potential for continental shelf regions to hold 3 to 4 times more Hg than previously estimated, it is critical to better constrain the fate of Hg over the estuarine-to-marine continuum [2].

Hg strongly binds to reduced sulfur sites in organic matter in aquatic environments [18], influencing its transport, transformations and bioavailability [7,19,20]. In riverine and estuarine systems, most Hg is bound to particles [2,21–24], and this is also observed in the Adour estuary [10,25]. The strong association of Hg with organic C has proven valuable in models constraining riverine Hg export to the ocean [2].

Distinct C stable isotopic signatures ($\delta^{13}C$) serves as a tracer for C origin and cycling, with terrestrial particulate organic matter typically exhibiting lighter values (i.e. -27‰ to -30‰) and phytoplankton-derived C (marine) showing heavier values (i.e.-20‰ to -25‰) [26].

Similarly, stable isotopic composition of Hg can be used constrain sources and/or characterize biogeochemical transformation processes in different matrices, such as marine sediments where Hg is ultimately buried [14,16,17,27–30]. Hg has seven stable isotopes, which undergo mass-dependent (MDF) and mass-independent fractionation (MIF) during partial biogeochemical processes, resulting in distinct signatures (δ^{202}Hg, Δ^{199}Hg, Δ^{200}Hg, Δ^{201}Hg, Δ^{204}Hg) that reflect different sources and/or processes [31,32]. While all studied biogeochemical processes [31,32] induce mass dependent fractionation (MDF, δ^{202}Hg), large mass-independent fractionation of odd Hg isotopes (odd-MIF, Δ^{199}Hg, Δ^{201}Hg) is predominantly of photochemical origin [33] due to the magnetic isotope effect (MIE) [34]. Another mechanism inducing odd-MIF, though of smaller magnitude, is the nuclear volume effect (NVE) [35]. In contrast, even-MIF (Δ^{200}Hg, Δ^{204}Hg) is considered a conservative tracer because it is thought to be exclusively generated by photochemical reactions in the upper troposphere and/or stratosphere [36,37]. Atmospheric Hg(0) and Hg(II) in precipitation exhibit distinct Δ^{200}Hg signatures, allowing the differentiation of atmospheric deposition pathways [38].

Here we investigate a gradient of surface sediments collected from the upstream Adour river estuary seaward including the initial 23.5 km of the Capbreton canyon (Bay of Biscay, Atlantic). High total Hg concentrations have been reported (> 500 ng g^{-1}) for the Capbreton canyon [5,39] which were found to be correlated with the carbon-rich fine fraction [5,39] and carbon stable isotopic composition (δ^{13}C) [5]. This continuum offers a unique opportunity to investigate Hg export and cycling along the transition zone from estuarine-to-marine environments. By combining stable isotopic composition of Hg and C, we aim to constrain geochemical processes and identify primary Hg sources along this unique land-ocean transition zone.

2. Material and Methods

2.1. Sampling Site

The Adour estuary and the adjacent Capbreton canyon are located in the south eastern Bay of Biscay (northeastern Atlantic Ocean, France). The Adour estuary is a mesotidal estuary within an urbanized area, while agriculture and livestock activities dominate the upstream and watershed resulting in different levels of anthropogenic impact [40]. The mean annual discharge is around 300 m^3 s^{-1} but can reach more than 2000 m^3 s^{-1} during brief flood events [10,25,41], which makes the Adour the third largest freshwater inflow into the Bay of Biscay [42]. The residence time of particles in the estuary is short (hours to days) compared to estuaries with a stronger marine influence [13,43–45]. It has been estimated that 75 % of the annual suspended matter flux occurs over 30 – 40 days during flooding events [13]. Although the Capbreton canyon has naturally been disconnected from the Adour river system in 1310 AD, the Adour remains the main sediment provider for the canyon, with active infill and particle remobilization processes still ongoing [46–48].

The Adour estuary and adjacent marine area has been extensively studied for Hg contamination and potential Hg transformations [5,10,25,40,41,44,49]. It has been shown that Hg water concentrations within the estuary decreased with anthropogenic Hg emissions over the past 20 years [25]. However, high levels of Hg (up to 975 ng g^{-1}) have been shown to accumulate on the slopes and terraces of the canyon, along with fine, organic-rich particles [5].

2.2. Sampling

The collected surface sediment samples represent an estuarine (Adour) to coastal-marine (Capbreton) gradient (Figure 1). The Adour samples (inter-tidal) were obtained during the MICROPOLIT project in three different sampling campaigns, in May 2017, September 2017, and January 2018 [41]. Capbreton samples were obtained during the HAPOGE oceanographic cruise within the first 23.5 km of the Capbreton and adjacent continental shelf [5]. Details on sampling have previously been published elsewhere [5,41]. In brief, Adour (n = 9) surface samples (0 – 5 cm) were collected at low tide (tidal

coefficient 81 to 108) by grab sampling while surface Capbreton (n = 24) samples were either collected with a Hybrid Remotely Operated Vehicle corer (HROV Ariane, Ifremer) or with a Van Veen grab sampler. Samples were stored in clean polyethylene bags and stored at -20°C rapidly after sampling.

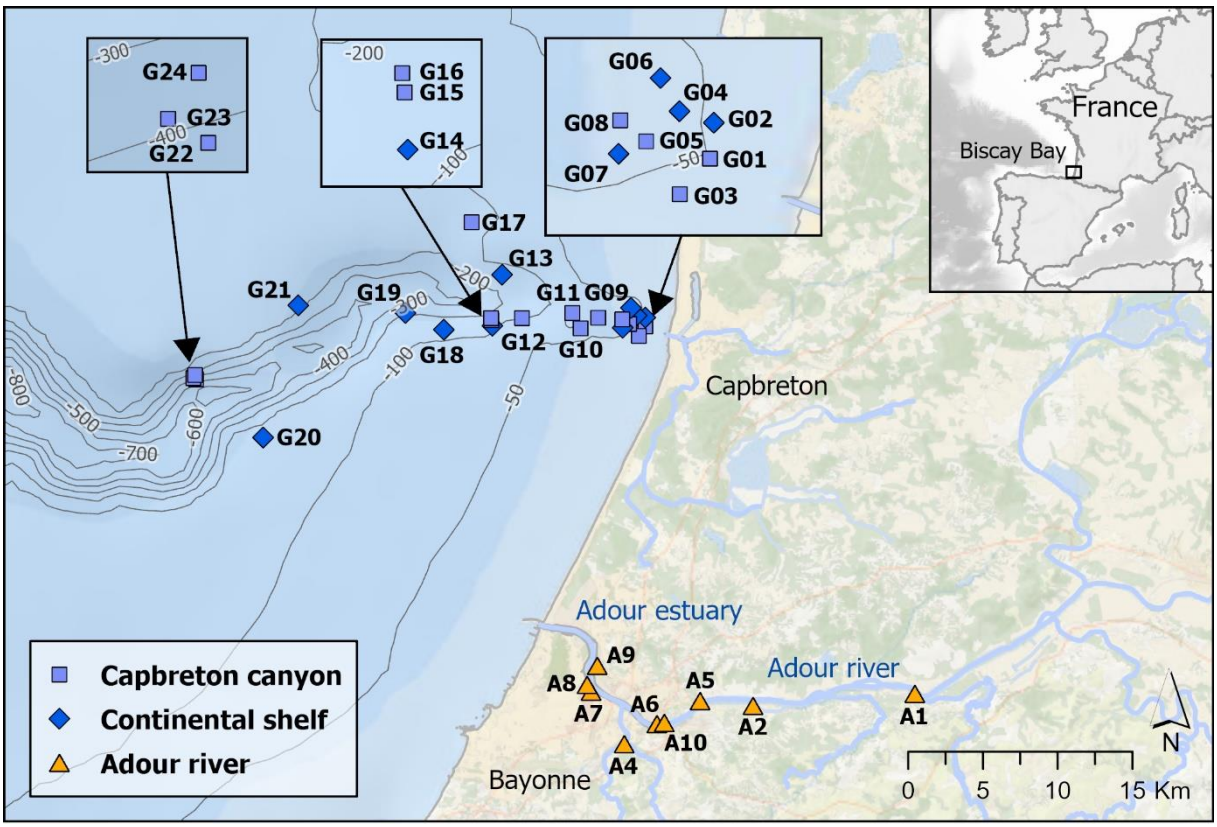

Fig 1. Sampling locations for the Adour river and estuary (referred to as “Adour” stations), and continental shelf and Capbreton canyon (referred to as “Capbreton” stations). Station A1 marks the limit of the Salinity intrusion.

2.3. Total Hg Concentration Measurements and Ancillary Parameters

All samples were homogenized and freeze-dried before further handling and ground with an agate mortar and pestle before digestion and total Hg analysis (THg). THg concentrations and ancillary parameters for Adour and Capbreton samples and the corresponding analytical procedures have been published elsewhere [5,41]. In brief, THg concentrations were determined on 50 – 100 mg of ground samples by atomic absorption spectrophotometry (AAS) on an Advanced Mercury Analyzer (AMA-254, Altec) for Adour samples. THg concentrations for Capbreton samples are the sum of MeHg and inorganic Hg determined by species-specific isotope dilution GC ICP-MS on sediment digests. Detection limit for THg in sediments based on three times the standard deviation (SD) of the digestion blank (Capbreton) was better than 0.07 ng g^{-1} dry weight or three times the SD of blank measurements with 3 ng g^{-1} dry weight (Adour). Accuracy and precision were determined by analyzing international certified materials of riverine and marine sediments (IAEA405/433, and BCR320R/580). For both analytical methods, mean recoveries/concentrations were within the 95 % confidence interval of certified values.

Total carbon (TC), particulate organic carbon (POC), carbon and nitrogen stable isotopes ($\delta^{13}C$, $\delta^{15}N$), the C:N ratio and grain size distribution were determined on all samples as described previously [5,41].

2.4. Hg Isotope Measurements

Hg stable isotopes were measured on digested samples with a cold-vapor multi-collector ICP-MS (Nu PLASMA Instruments, Wrexham UK) following the method described in previous studies [50,51]. Dry, finely ground sediment samples were pre-digested with 3 mL HNO_3 (69 – 70 %, Suprapure) and 1 mL HCl (33 – 36 %, Suprapure) for a minimum of 8 hours before digestion on a Hot Block for 4 hours at 85°C. After addition of 1 mL of H_2O_2 (Ultrapure), this was followed by a second cycle of digestion of 2 hours. Samples were centrifuged (10 min, 4500 rpm) and supernatant recovered and stored at +4°C until final dilution to 0.5 or 1 ng g-1 with 2 % HNO_3 (69 – 70 %, Suprapure) for isotopic measurements.

To account for sample heterogeneity, replicate digestions and analyses were performed approximately every 10 samples.

Total Hg isotopic composition was measured for the six most abundant stable Hg isotopes (^{198}Hg, ^{199}Hg, ^{200}Hg, ^{201}Hg, ^{202}Hg, ^{204}Hg) relative to the bracketing standard NIST SRM 3133. Mass-bias was corrected via simultaneous introduction of NIST SRM 997 thallium by nebulization. Results are reported in the conventional δ-notation, representing the deviation from the bracketing standard in permil (‰) where *xxx* represents Hg isotope masses (Eq 1).

(Eq 1) $$\delta^{xxx}Hg = \left(\frac{\left(\frac{^{xxx}Hg}{^{198}Hg}\right)_{sample}}{\left(\frac{^{xxx}Hg}{^{198}Hg}\right)_{SRM3133}} - 1 \right) \times 1000$$

MIF values are expressed by capital delta notation (Δ), expressing the difference between the measured values of $\delta^{199}Hg$, $\delta^{200}Hg$, $\delta^{201}Hg$ and $\delta^{204}Hg$, and those predicted from $\delta^{202}Hg$ using the kinetic MDF law [33] where β^{xxx} is 0.2520, 0.5024, 0.7520 and 1.4930 for ^{199}Hg, ^{200}Hg, ^{201}Hg and ^{204}Hg, respectively (Eq 2).

(Eq 2) $$\Delta^{xxx}Hg = \delta^{xxx}Hg - (\beta^{xxx} \times \delta^{202}Hg)$$

The analytical uncertainty was assessed by repeated analysis of the UM-Almaden reference material and procedural standards (Table SI 1) over different analytical sessions at Hg concentrations corresponding to the samples. The mean values of for the UM-Almaden reference material agreed with reported reference values [52]. Reported analytical uncertainties in all Figures were based on the highest 2 SD obtained on reference material or procedural SRMs (0.18 ‰ for δ^{202}Hg, 0.12 ‰ for Δ^{199}Hg, 0.09 ‰ for Δ^{200}Hg, and 0.12 ‰ for Δ^{201}Hg). Sample heterogeneity, expressed as 1SD of replicates (n = 2 or 3), was similar or below the analytical uncertainty, except for δ^{202}Hg of two Adour samples (A8 and A9) from the sampling campaign conducted in September (Table SI 2).

2.5. Hg Burial rates

The Capbreton canyon is a large incision in the continental shelf characterized by its high sediment export from the land to the deep ocean, where elevated accumulation rates (more than 1 cm yr^{-1}) are observed on terraces [39,48]. To estimate Hg burial rates on the Capbreton Canyon terraces, we used dry bulk density and surface THg concentrations for two sediment cores (G09, G23), applying conservative sedimentation rates of 0.19 and 0.45 cm yr^{-1} from literature for the Capbreton Canyon (see SI section 1.3 for details).

2.6. Statistical Testing and Binary Mixing Model for Source and Process Tracing

Statistical analysis was conducted in R using the rstatix package. Spearman correlations were calculated, and differences between sampling groups and seasons were assessed using the non-parametric Kruskal-Wallis test, followed by Dunn's post hoc test.

All binary mixing models were calculated following generalized equations Eq 3 and Eq 4:

(Eq 3) $$f_{pool\ A} = \frac{\sigma_{sample} - \sigma_{pool\ B}}{\sigma_{pool\ A} - \sigma_{pool\ B}}$$

(Eq 4) $$f_{pool\ A} + f_{pool\ B} = 1$$

Where $f_{pool\ A}$ and $f_{pool\ B}$ are the estimated contributions of pool A and pool B to the sample, $\sigma_{pool\ A}$ and $\sigma_{pool\ B}$ are the corresponding isotopic signatures of pool A and pool B, and σ_{sample} is the isotopic signature of the sample. We used Δ^{200}Hg to calculate atmospheric Hg(0) (pool A) and precipitation-derived Hg (pool B), δ^{202}Hg to calculated land-derived Hg (pool A) and Hg from direct atmospheric deposition (pool B), and δ^{13}C to calculate terrestrial C (pool A) and marine C (pool B).

After obtaining the contributions of atmospheric Hg(0) and precipitation-derived Hg (see SI section 1.4 for details on endmember) based on Δ^{200}Hg, these were subsequently used to calculate the excess Δ^{199}Hg ($\Delta^{199}Hg_{exc}$; Eq 5). The $\Delta^{199}Hg_{exc}$ represents Δ^{199}Hg that cannot be explained by the mixing of Hg(0) and precipitation-derived Hg alone.

(Eq 5) $\Delta^{199}Hg_{exc} = \Delta^{199}Hg_{sample} - \left(f_{Hg(0)} \times \Delta^{199}Hg_{Hg(0)} + \left(1 - f_{Hg(0)}\right) \times \Delta^{199}Hg_{precipitation}\right)$

Where $\Delta^{199}Hg_{sample}$ is the $\Delta^{199}Hg$ in the sample, and $\Delta^{199}Hg_{(Hg(0))}$ and $\Delta^{199}Hg_{Precipitation}$ are $\Delta^{199}Hg$ values in the Hg(0) and precipitation endmembers, respectively.

Uncertainties in calculated $f_{pool\,A}$, $f_{pool\,B}$, and $\Delta^{199}Hg_{exc}$ were evaluated through Monte Carlo simulations (100 000 iterations) and assuming normal uncertainty distributions for all parameters partaking in Eq 3, Eq 4, and Eq 5. This is further described in the supplementary information (section 1.5), and the used R code can be freely accessed under https://github.com/AlkuinKoenig/BinaryMixing_MonteCarlo.

3. Results & Discussion

3.1. THg concentrations, stable isotopic composition of C and Hg

Table 1 summarizes THg concentrations, ancillary parameters (e.g. fine fraction, $\delta^{13}C$, $\delta^{15}N$), and Hg stable isotopic composition for Adour and Capbreton sampling groups. Ancillary parameters and THg concentrations have been reported in detail elsewhere for both Adour [41] and Capbreton samples [5].

THg concentrations were significantly lower ($p < 0.05$) in Adour samples (median = 75 ng g^{-1} d.w., n = 27) than in Capbreton samples (median = 138 ng g^{-1} d.w., n = 24). The majority of Capbreton samples (16 out of 24) and several Adour samples with a high urban influence (May: A4, A6; September: A4, A6, A7; January: A6), had THg concentration above the 90th percentile (94.4 ng g^{-1} d.w.) of selected literature data (marine and estuarine sediments for which THg and isotopic composition data were available; Figure SI 2). While geogenic inputs have previously been shown to be insignificant in Pyrenean lakes within the Adour catchment [53], the Adour estuary is anthropogenically impacted, with declining Hg burdens corresponding to decreasing Hg emissions [25]. Anthropogenic point

sources (e.g. station A6 near a sewage treatment plant) [25,41] are likely responsible for slightly elevated THg concentrations in Adour samples while high THg in Capbreton samples have previously explained by enrichment of Hg on fine, organic-rich particles [5]. Indeed, we find a significant positive correlation (Spearman, $p < 0.05$, Figure SI 3) between THg with $\delta^{13}C$ ($\rho = 0.58$) (Figure 3A), and the fine fraction ($\rho = 0.51$), for the whole dataset (Adour and Capbreton), whereas a significant correlation (Spearman, $p < 0.05$) between THg and POC could only be established (both $\rho = 0.67$, Figure SI 4) when separating the two sampling groups [5,41]. This confirms that high THg concentrations farthest from the coast are not due to direct anthropogenic point sources in the estuary and are driven by fine particles rather than just POC.

A significant difference ($p < 0.05$) between Adour and Capbreton samples was found for POC, the C:N ratio, $\delta^{13}C$ and $\delta^{15}N$, but not for the fine fraction. There was, however, a significant ($p < 0.05$) difference in the fine fraction between Capbreton shelf (median = 37.6 %) and canyon samples (median = 70.2 %) (Figure SI 5). This illustrates that coarser particles are mainly deposited near shore, while finer particles are preferentially transported seaward and trapped in the canyon [5]. The lower $\delta^{13}C$ (and $\delta^{15}N$, C:N ratio) of Adour samples is consistent with typical values for terrestrial organic matter (Figure 2), while the higher $\delta^{13}C$ (and $\delta^{15}N$, C:N ratio) of Capbreton samples all together indicate a greater proportion of marine organic matter (Figure 2, Figure SI 5) [54]. This confirms that, based on the major carbon sources, our samples are representative of a terrestrial to marine continuum.

Despite the differences in THg concentrations and/or ancillary parameters, no significant difference ($p < 0.05$) for Hg stable isotopic composition was found between Adour samples collected in different seasons (Figure SI 6), nor between samples collected in the Capbreton canyon and its adjacent shelf (Figure SI 5). We therefore assigned all sediment samples to one of two groups, estuarine (Adour) or coastal-marine (Capbreton), based on their sampling location (Figure 1).

The observed Hg stable isotopic composition in this study for $\delta^{202}Hg$, $\Delta^{199}Hg$, $\Delta^{200}Hg$ and, $\Delta^{201}Hg$ were on average ± 1SD, -0.70 ± 0.21 ‰ (range = -1.06 to - 0.27 ‰), -0.05 ± 0.05 ‰ (range = -0.14 to 0.08

246 ‰), 0.0 ± 0.03 ‰ (range = -0.06 to 0.10 ‰) and -0.07 ± 0.05 ‰ (range =-0.18 to 0.04 ‰), respectively.
247 Observed Hg isotopic signatures in the Adour-Capbreton sediments exhibited a relatively small range
248 and were within literature values (Figure SI 2). A significant ($p < 0.05$) difference between Adour and
249 Capbreton samples was found only for $\delta^{202}Hg$ and $\Delta^{201}Hg$, with heavier values recorded in Capbreton
250 samples. The most notable, significant correlation (Spearman, $p < 0.05$) for Hg and C isotopic
251 composition along the estuarine-to-marine continuum was observed between $\delta^{202}Hg$ and $\delta^{13}C$ (ρ =
252 0.78, Figure 2B), showing an enrichment in heavier isotopes for more marine $\delta^{13}C$ signatures.

253 In summary, along the estuarine-to-marine continuum from upstream to Capbreton canyon samples
254 (Figure 2C), we observe an overall shift towards higher THg concentrations, heavier MDF ($\delta^{202}Hg$) and
255 odd-MIF signatures ($\Delta^{199}Hg$, $\Delta^{201}Hg$), and a transition from mainly terrestrial carbon sources to a
256 greater contribution of marine carbon sources (Figure 2).

257

	Adour	Capbreton
Ancillary Parameter		
THg d.w. (ng g^{-1})	75 (61 – 90) **	138 (85 – 290) **
Fine fraction (%)[a]	69.2 (51.2 – 77.5)	58.2 (40.1 – 90.2)
POC (%)	3.01 (1.45 – 3.93) **	1.4 (0.67 – 1.89) **
TC (%)	3.54 (1.69 – 4.74)	2.78 (1.84 – 3.59)
C:N	11.66 (11.05 – 12.22) **	12.4 (12.1 – 13.0) **
$\delta^{13}C$ (‰)	-27.3 (-27.6 – -27.0) **	-25.6 (-25.8 – -24.4) **
$\delta^{15}N$ (‰)	4.2 (3.9 – 4.4) **	5.0 (4.7 – 5.3) **
Hg Stable Isotopic Composition		
$\delta^{202}Hg$ (‰)	-0.82 (-0.96 – -0.75) **	-0.52 (-0.62 – -0.47) **
$\Delta^{199}Hg$ (‰)	-0.07 (-0.1 – -0.04)	-0.03 (-0.07 – 0)
$\Delta^{200}Hg$ (‰)	0.01 (-0.1 – 0.02)	0.00 (-0.02 – 0.02)
$\Delta^{201}Hg$ (‰)	-0.09 (-0.11 – -0.07) **	-0.04 (-0.08 – -0.01) **

Table 1. Overview of Ancillary Parameters and Hg stable isotope composition for Capbreton and Adour. Median values are given and 25th and 75th percentile in brackets. [a]for Capbreton <0.63 µm and for Adour <0.50 µm. **Significant difference ($p < 0.05$) between groups (Kruskal-Wallis, Dunn's post-hoc)

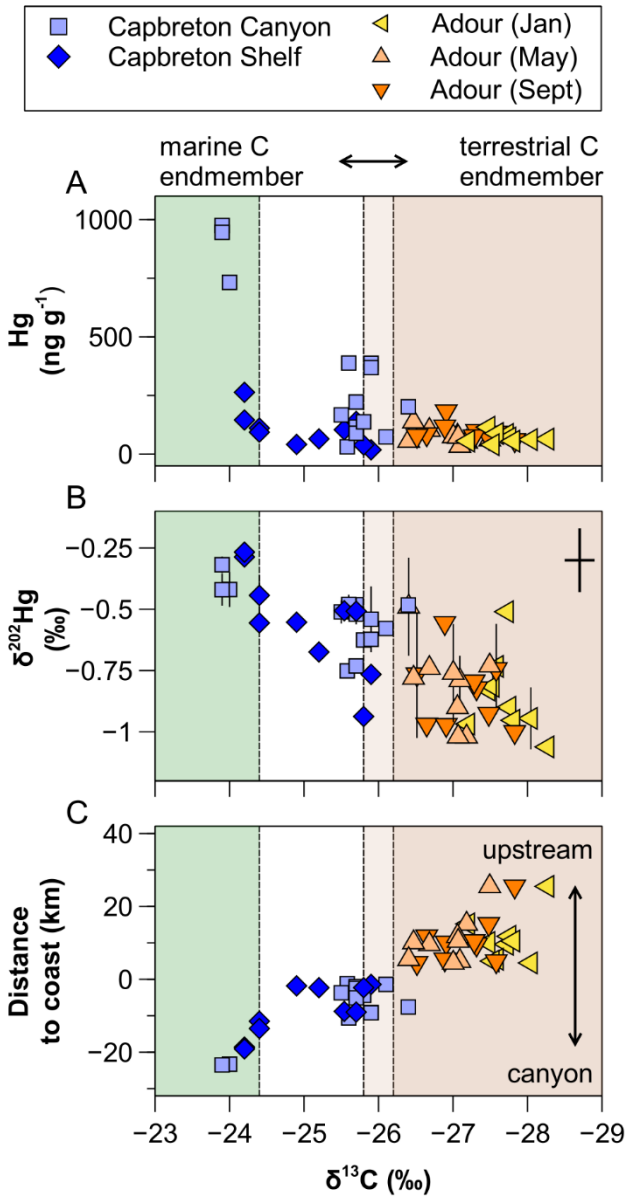

261

262 Figure 2. THg concentration, MDF (δ^{202}Hg), and distance to the coast over δ^{13}C for Capbreton and
263 Adour samples. For Adour samples, the distance to the coast was measured along the Adour River to
264 its mouth, for Capbreton samples the distance to the coast was used. Shaded areas indicate typical
265 δ^{13}C values for phytoplankton (marine, in green) and riverine-estuarine particulates (terrestrial, in
266 brown) based on published data [55] (for details see Figure SI 7). Average values of replicates are
267 plotted with error bars (1SD). The cross in the upper right corner of B panel represents the analytical
268 precision (2SD) for δ^{202}Hg and δ^{13}C based on multiple analyses of procedural standards.

269

3.2. Influence of biogeochemical processes on Hg stable isotopes

Biogeochemical processes can affect both the MDF (δ^{202}Hg) and odd-MIF (Δ^{199}Hg, Δ^{201}Hg) isotopic composition of Hg, potentially overprinting source signatures. Two mechanisms are known to influence the odd-MIF, the nuclear volume effect (NVE) [35], and the magnetic isotope effect (MIE) [34]. Elemental Hg evaporation [56,57] and equilibrium Hg-thiol complexation [58] are found to have a NVE with experimentally determined Δ^{199}Hg/Δ^{201}Hg slopes of 1.65 – 2.0 and 1.56, respectively. The MIE is found for example during photo-reactions of aqueous Hg, with experimentally determined Δ^{199}Hg/Δ^{201}Hg slopes of 1.00 – 1.3 [33,59,60]. Given that MeHg typically represent a small fraction of THg (<1%) in Adour and Capbreton sediments [5,40], fractionation related to methylation of Hg(II) [51] or photo-demethylation of MeHg [33] can be neglected for our samples.

As shown in Figure 3, no clear trends were observed between the Adour river and the coastal samples along the 1.00 or 1.56 Δ^{199}Hg/Δ^{201}Hg slope, characteristic for MIE or NVE respectively (Figure 3B). This, together with the narrow range of odd-MIF (Δ^{199}Hg = -0.14 – 0.08 ‰), suggests a limited influence of photochemical reduction of Hg before incorporation into sediments for both Capbreton and Adour samples. This is in line with previous studies, which observed insignificant odd-MIF in open seawater beyond the signatures resulting from the mixing of two atmospheric Hg(0) and Hg(II) sources [27].

In contrast, a difference between estuarine and marine sediments with a shift towards heavier odd-MIF signatures along the ~1.00 Δ^{199}Hg/Δ^{201}Hg slope due to enhanced photo-reduction in marine compared to estuarine waters (Figure 3B) had previously been observed in the subtropical South China Sea [17]. For our study area, however, it has been demonstrated that ~75% of the annual flux of suspended solids from the Adour river occurs during flooding events, mobilizing large particles that rapidly settle [13]. During such events, the short residence time and increase in turbidity can limit photochemical processes [10].

To further address if photochemical or processes impacted Δ^{199}Hg of our samples, we evaluate the excess of Δ^{199}Hg ($\Delta^{199}Hg_{exc}$), where $\Delta^{199}Hg_{exc}$ represents the deviation of Δ^{199}Hg from the expected

Δ^{199}Hg through mixing of Hg(0) and precipitation endmembers. The presence of significant positive or negative $\Delta^{199}Hg_{exc}$ would suggest a significant influence of additional pre- or post-depositional processes affecting the odd-MIF and MDF Hg isotopic composition [27]. Here, we observe neither a significant (α = 0.05) $\Delta^{199}Hg_{exc}$ for any Adour or Capbreton sample (see Figure SI 8, Figure SI 9), nor a significant difference (Kruskal-Wallis, Dunn's post-hoc) in mean $\Delta^{199}Hg_{exc}$ between Adour and Capbreton sample groups. The absence of such is consistent with a significant (Spearman, $p < 0.05$) correlation between Δ^{200}Hg and Δ^{199}Hg (ρ = 0.63), suggesting that the observed variation of Δ^{199}Hg can be explained by the mixing of two atmospheric sources of Hg (Hg(0) and precipitation-derived Hg) alone.

That said, there are also other processes that may influence δ^{202}Hg values while inducing only minor or negligible Δ^{199}Hg fractionation. One example is equilibrium Hg-thiol complexation, which enriches heavy Hg isotopes in the residual dissolved pool with a fractionation factor of ~0.5 ‰ for δ^{202}Hg and a smaller fractionation (<0.1‰) for Δ^{199}Hg [58]. Given the complexity of our study system and the limitation of our data on sediments, the extent to which Hg-thiol complexation affects the isotopic signature of the dissolved Hg pool remains uncertain.

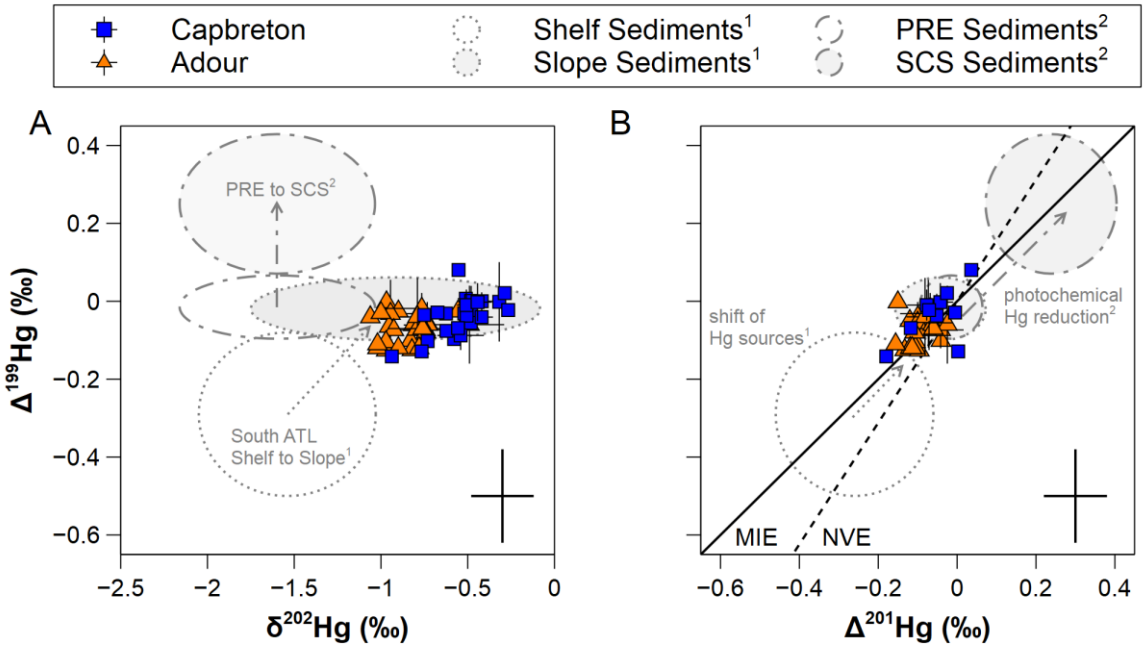

310

311 Figure 3. Δ^{199}Hg over A) δ^{202}Hg and B) Δ^{201}Hg in for Adour and Capbreton samples and selected
312 literature data for the South Atlantic (ATL), Pearl River Estuary (PRE) and South China Sea (SCS). B) The
313 full line indicates the slope of 1 which is typical of photo-reduction of inorganic Hg (MIE) and the
314 dashed line the slope of 1.56 which is typical for equilibrium thiol-complexation (NVE). Average values
315 of replicates are plotted with error bars (1SD), the crosses in the lower right corner represent the
316 analytical precision (2SD) based on multiple analyses of procedural standards.[1]Araujo et al. 2017 [14]
317 and [2]Yin et al. 2015 [17].

3.3. Hg Burial Rates and Hg Accumulation on Fine Particles

The Hg burial rates were estimated for two samples located on terraces but at different distances to the coast. For station G09 at the head of the canyon (3.7 km from the coast, $\delta^{13}C$ of -25.5 ‰) receiving both terrestrial and marine C, and station G23, one of the farthest stations from the coast (23.5 km from the coast, $\delta^{13}C$ of 23.9 ‰), receiving mostly marine C based on $\delta^{13}C$. Following THg concentrations, estimated Hg burial rates were lower near the coast (G09, 197 – 466 µg Hg m^{-2} yr^{-1}) than for farther off-shore canyon terraces (G23, 927 – 2196 µg Hg m^{-2} yr^{-1}). Hg burial rates at the canyon head are 5 to 12 times higher than median global shelf (39 µg Hg m^{-2} yr^{-1}) [28] burial rates, while rates at the distal canyon terraces are 24 to 56 times higher, demonstrating an unprecedently high accumulation of Hg in the Capbreton canyon terraces.

Maximum THg concentration (> 500 ng g^{-1} d.w.), exceeding concentrations reported in contaminated shelf sediments including the Bohai Sea, China (574 ng g^{-1}) [61], were found furthest from the coast in Capbreton samples [5,39]. Azaroff et al. 2019 already hypothesized that these high Hg concentrations may be controlled by the accumulation of Hg on fine particles [5], which efficiently transport Hg into the Capbreton Canyon , acting as a sediment trap. They could, however, give no insight about the origin of the high Hg concentrations in these samples.

Based on our Hg stable isotopic composition observations, we can exclude a point source contamination as a possible reason for the highly concentrated Capbreton samples (above 732 ng g^{-1}). Indeed, we do not find a significant difference ($p < 0.05$) in Hg isotope composition ($\delta^{202}Hg$, $\Delta^{199}Hg$, and $\Delta^{200}Hg$) between highly (above 732 ng g^{-1}, n = 3) and low-concentrated (n = 3) Capbreton sediments of the marine $\delta^{13}C$ endmember (above -24.4 ‰) (Figure SI 10). This suggests that the Hg in both the high and low-concentration marine-endmember samples originates from the same pool, raising questions about the underlying processes leading to elevated THg concentrations in fine particles.

Both THg concentrations and $\delta^{202}Hg$ isotopic composition for Capbreton samples were significantly ($p < 0.05$) correlated with water depth and $\delta^{13}C$ (thus distance to the coast; Figure 2, Figure SI 11).

However, the absence of a significant correlation between the fine fraction and Hg isotopic composition (δ^{202}Hg, Δ^{199}Hg, Δ^{201}Hg; Figure SI 11) suggests that δ^{202}Hg variability cannot be explained by particle size-dependent isotopic fractionation during particle transport.

Efficient accumulation of Hg on fine particles may be explained by the longer settling times of finer particles in the canyon, which enables a proportionally greater organic carbon remineralization and higher Hg concentrations due to "regenerative scavenging", where Hg is rapidly re-scavenged onto particulate organic matter [4,28]. In addition, frequent resuspension and transport of fine organic-rich particles through gravity-driven mass movements within the canyon may allow for additional Hg accumulation on fine particles [46–48]. Similar observations have been reported, far from direct anthropogenic influence, for trench sediments with high Hg concentrations (up to 400 ng g^{-1}) [28,62]. Given that Hg sedimentation to deep oceanic sediments is one of few ways to remove Hg from the marine biogeochemical cycle [63], further investigation into the underlying processes is needed in the future.

3.4. Discrimination of Potential Hg Sources to Estuarine-to-Marine Sediments

In our system, Hg mainly originates from vegetational uptake (atmospheric Hg(0)), urban influence, and precipitation (mostly Hg(II)). Both are stored in soils and enter the river system through runoff before being exported to the coastal ocean [25,53]. In addition, Hg may be deposited to the ocean via direct atmospheric deposition of Hg(0) (dry) and Hg(II) (wet and dry) [27]. Terrestrial Hg, i.e. Hg(0) sequestered by foliage and subsequently oxidized, is imprinted with a significant (>2 ‰) shift towards lighter δ^{202}Hg values [64], while post-depositional processes and Hg re-emission may induce a significant shift in both δ^{202}Hg and Δ^{199}Hg in soils or atmospheric accumulators [64].

The potential sources of Hg in sediments for our study area are compiled in Figure 4 along with local isotopic signatures for lichens, mosses [65], soils [65], total gaseous mercury (here assumed equal to Hg(0)), precipitation [38,66], and the global open ocean [27]. Dry Hg(0) deposition typically dominates Hg signatures in soils and atmospheric accumulators, such as lichens and mosses. This was also established for local (catchment area of the Adour river) lichens and mosses in the western Pyrenees with an Hg(0) contribution of ~80 % on average (Figure SI 9) (Barre et al. 2018, 2020). A considerable deviation from the linear regression of Δ^{199}Hg and Δ^{200}Hg signatures for Hg(0) and precipitation suggests that most local soil, lichen, and some moss samples were affected by post-depositional processes (Figure 4B). This is exemplified by a mean negative $\Delta^{199}Hg_{exc}$ for soils and lichens (Figure SI 9), while $\Delta^{199}Hg_{exc}$ for mosses was more variable (Figure SI 8) [65].

For Adour and Capbreton sediment samples, however, we do not observe such deviation of Δ^{199}Hg from the theoretical mixing between Hg(0) and precipitation-derived Hg (Figure 4D). This is in line with the previously established absence of $\Delta^{199}Hg_{exc}$. The absence of $\Delta^{199}Hg_{exc}$ in Adour sediments suggests that Hg in estuarine sediments has not undergone such post-depositional processes. However, it cannot be excluded that another process or source may obscure the $\Delta^{199}Hg_{exc}$ signature, or that most lichens, and to some extent soils samples do not represent our estuarine Hg endmember found in Adour sediments (Δ^{199}Hg, possibly δ^{202}Hg).

We propose that the observed shift towards heavier $\delta^{202}Hg$ with marine $\delta^{13}C$ reflects a gradual shift from land-derived i.e. terrestrial Hg which has mainly undergone vegetational uptake with possible anthropogenic impact, to a marine Hg signature from direct atmospheric deposition of Hg(II) (wet and dry) and Hg(0) (roughly 1:1) [27].

We find that Adour sediment samples lack $\Delta^{199}Hg_{exc}$ and have heavier $\delta^{202}Hg$ signatures than reported for most soils, lichens and mosses of the Adour catchment area [65,67]. Barre et al. (2018) reported distinct $\delta^{202}Hg$ and $\Delta^{199}Hg$ in lichens based on land uses. While background lichens had lightest $\delta^{202}Hg$ (-1.99 ± 0.45 ‰) and $\Delta^{199}Hg$ values (-0.32 ± 0.10 ‰), heavier signatures were found for lichens sampled within the industrial sector ($\delta^{202}Hg$ =-1.10 ± 0.35 ‰, and $\Delta^{199}Hg$ = -0.28 ± 0.07 ‰) and for lichens directly impacted by the steel industry ($\delta^{202}Hg$ -0.68 ± 0.32 ‰, and $\Delta^{199}Hg$ = -0.10 ± 0.18 ‰) (Figure 4A) [67]. The Hg isotopic composition in Adour sediments may thus reflect a significant urban influence potentially imprinted in surrounding soils, consistent with the proximity of the sampling sites to urban areas and industrial facilities [41]. However, based on our data, we cannot rule out the influence of marine Hg on Adour sediments in the highly dynamic estuarine system [45], potentially obscuring lighter $\delta^{202}Hg$ and $\Delta^{199}Hg$. All Adour sediments were influenced by displacement and frequent resuspension [68], as the upstream sample (A1) of this study was collected at the limit of the salinity intrusion.

Our hypothesis aligns with previous sediment studies on estuarine to marine gradients with similar observations [14,16]. It is also supported by a study on Hg stable isotopes in filtered (0.45 µm) waters over an estuarine to pelagic gradient (South China Sea) which reported a trend towards heavier $\delta^{202}Hg$ (MDF) along with a decrease in total Hg further from the coast [69], while urban influenced coastal waters of the Mediterranean had $\delta^{202}Hg$ and $\Delta^{199}Hg$ close to 0 (Figure SI 12) [27]. Overall, this aligns with our observations: as terrestrial carbon becomes increasingly diluted with distance from the coast, so does land-derived Hg (- MDF), while marine carbon is associated with a distinct, heavier oceanic Hg pool (+ MDF) (Figure 2B, Figure 4C).

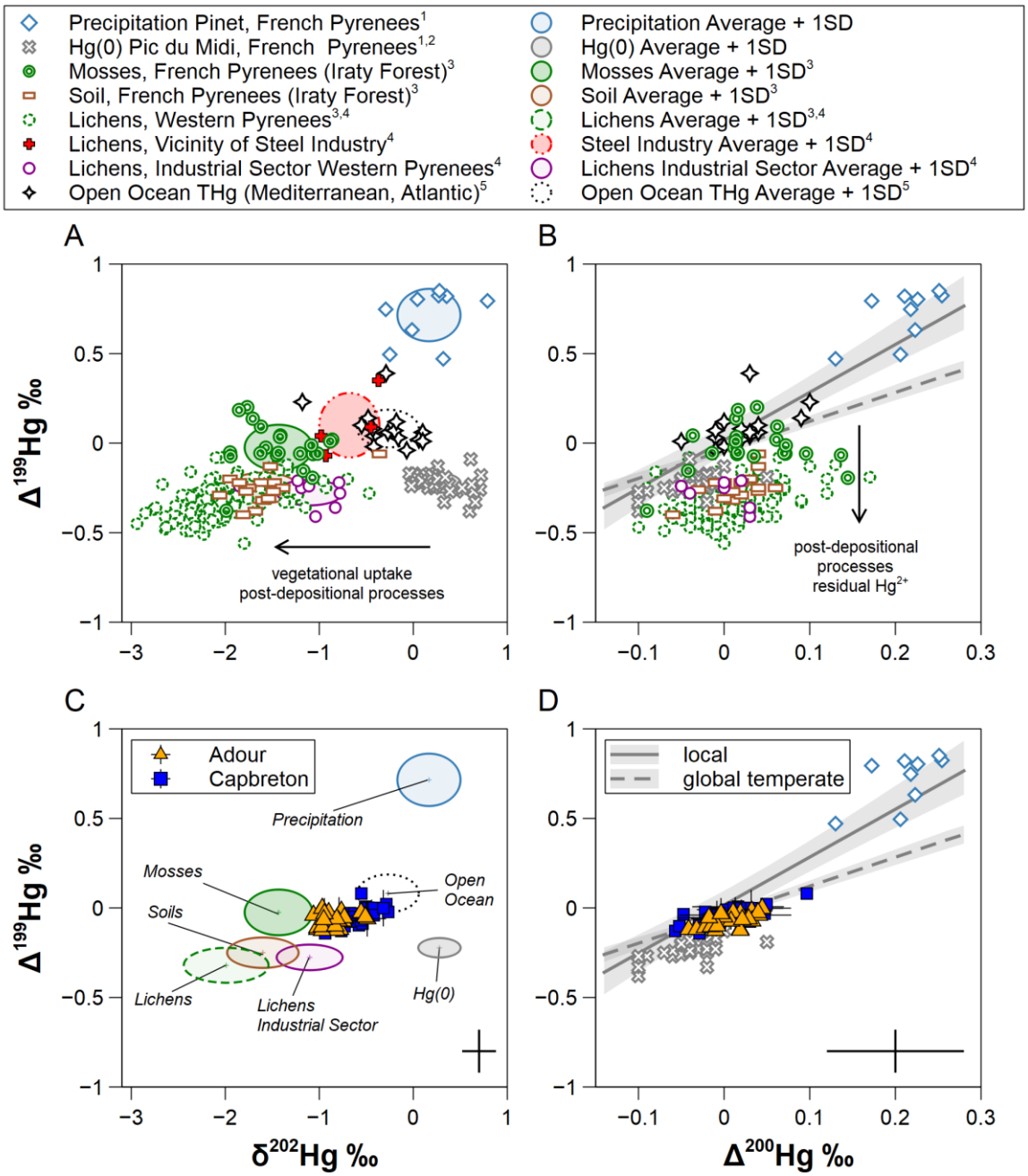

406 Figure 4. Potential Hg sources for sediments along an estuarine-marine gradient based on literature.
407 A, B) δ^{202}Hg vs. Δ^{199}Hg signatures for direct atmospheric sources (Hg(0) and precipitation-derived Hg),
408 soils, bioindicators and open ocean observations. A vegetational uptake shift in δ^{202}Hg (- MDF) is
409 reflected in lichens, mosses and soils with varying degree of industrial contamination. B, D) The grey
410 line represents the theoretical linear mixing (shaded area: 95 % confidence interval) between Δ^{200}Hg
411 and Δ^{199}Hg for Hg(0) and precipitation, based on literature from the Pyrenees, while the dashed line
412 represents the York fit (shaded area: 95 % confidence interval) for global observations in temperate
413 background sites (SI section 1.4). Deviations from the theoretical mixing line indicate shifts in Δ^{199}Hg
414 of residual Hg(II) due to post-depositional redox processes. C, D) Average values of replicates are
415 plotted with error bars (1SD). The crosses represent the analytical precision (2SD) based on multiple
416 analyses of procedural standards. [1]Enrico et al., 2016 [38], [2]Fu et al., 2016 [66], [3]Barre et al., 2020 [65],
417 [4]Barre et al., 2018 [67], and [5]Jiskra et al., 2021 [27].

418

3.5. Implications for Hg Source Apportionment in Coastal Marine Systems

Our data suggest that biogeochemical processes had a minor influence on Hg isotopic composition and that the observed differences in δ^{202}Hg along the estuarine to coastal-marine continuum are best explained by a mixing of different Hg sources. To decipher the main sources of Hg in the study area, we applied a two-endmember mixing model. The two endmembers were defined as land-derived Hg i.e. derived from vegetational uptake and anthropogenic impact (lichens industrial sector), and direct atmospheric deposition of Hg (open ocean).

We find a significant difference between sampling groups (Figure SI 13), with a higher land-derived Hg contribution in Adour (70 ± 19 %) compared to Capbreton samples (33 ± 19 %). While the estimated fraction of terrestrial Hg naturally depends on the defined endmembers, our results illustrate the progressive dilution of land-derived Hg along the estuarine-marine sediment gradient.

It is notable that, if approximately 70% of Hg in sediment samples from the Adour estuary is land-derived, around 30 % is not. This may be explained by a direct anthropogenic (urban) influence in these sediments, the transport of marine Hg from the shelf into the Adour estuary (for instance through tidal pumping), or a combination of both. However, due to the absence of Hg isotopic composition difference in the “direct anthropogenic” and “marine” pools for our study area (both + MDF, as obtained from literature), we are not able to resolve this question here.

We give a conservative estimate on land-derived Hg burial rates ($Hg_{land\text{-}derived}$), considering the established minimum Hg burial rates at the Canyon head (G09: 97 µg Hg m^{-2} yr^{-1}) and the farthest Canyon terrace (G23: 927 µg Hg m^{-2} yr^{-1}), and the respective mean land-derived Hg contribution. The slightly higher mean contribution of direct atmospheric deposition for G23 (29 %) than for G09 (18 %) is clearly offset by higher burial rates on terraces further in the canyon, amounting to ~57 µg $Hg_{land\text{-}derived}$ m^{-2} yr^{-1} at the canyon head and ~165 µg $Hg_{land\text{-}derived}$ m^{-2} yr^{-1} in farthest terraces. This underscores that the canyon functions as a major sediment trap for both land-derived and marine Hg.

To examine the joint behavior of Hg and C along this estuarine-to-marine continuum, we selected endmembers based on spatial location (Figure 1, Figure 2C), with the upstream sample A1 (average of

three seasons) for the land-derived Hg and C endmembers, while samples G22-G24, farthest from the coast and with the highest THg concentrations, serve as the marine endmembers. We find a linear relationship close to 1 (Figure 5) between land-derived Hg and terrestrial C fractions calculated from Hg and C isotopes, indicating that Hg and C are being jointly diluted in our system. In agreement with the short residence time of suspended particulate matter in the estuary [43,68], the Hg and C relationship indicates that both terrestrial Hg and C are efficiently exported from the estuary and buried into coastal and canyon sediments.

Our results suggest that the fraction of terrestrial carbon in a coastal sediment sample may give direct insights into the fraction of land-derived Hg it contains. This implies that the amount of land-derived Hg could be adequately estimated by knowing the THg concentration and the carbon isotope composition alone, reducing the reliance on Hg isotope composition measurements. On one hand, this could enable new sampling campaigns and field studies with a greater temporal or regional coverage, as measuring carbon isotopes is significantly simpler and far less costly than measuring Hg isotopes. On the other hand, such a relationship could allow the scientific community to leverage existing databases containing joint observations of Hg concentration and carbon isotope composition to estimate land-derived Hg inputs into coastal oceans worldwide. Before that, however, it is imperative to confirm the validity of this relationship between terrestrial C and land-derived Hg for other coastal regions outside our study area.

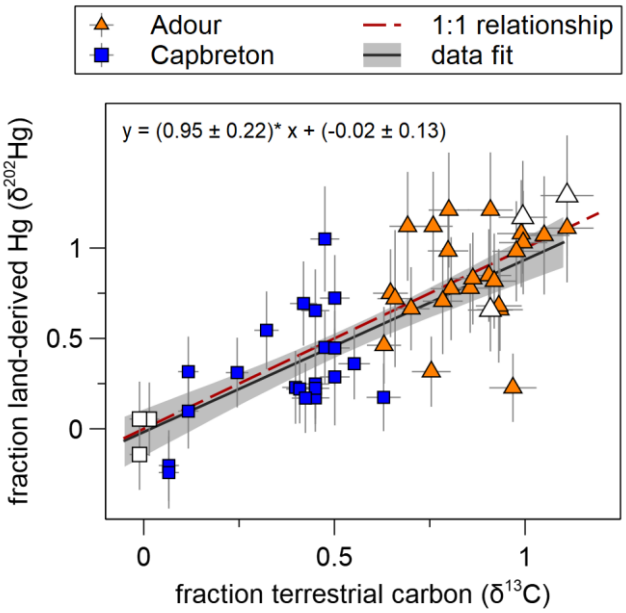

463

464 Figure 5. Binary-mixing model based on δ^{202}Hg and δ^{13}C values along the estuarine-to-marine
465 gradient suggests joint sedimentation of land-derived Hg and terrestrial C. Endmember samples (A1
466 all seasons, G22, G23, G24) selected based on their spatial distribution, are displayed without color.
467 Error bars depict propagation uncertainties (50 % confidence interval) from analytical measurement
468 uncertainties (δ^{202}Hg and δ^{13}C) and the variability between endmember samples (standard error of
469 mean). The continuous line represents the best fit to all while the shaded grey area indicates the
470 2.5th and 97.5th confidence interval of the fit.

Acknowledgements

We thank the crew of the INSU-CNRS research vessel Côte de la Manche for their support during marine sediment sampling, and Sylvain Bérail for his assistance with mercury isotopic analyses in the laboratory. This work was supported by the European Union and the Adour-Garonne Water Agency through the MICROPOLIT project via the European Regional Development Fund (ERDF – MICROPOLIT project). This research is also part of the GMOS-Train network, funded by the European Union's Horizon 2020 research and innovation program under the Marie Skłodowska-Curie grant agreement No. 860497. Additional support was provided by the Energy and Environment Solutions (E2S-UPPA) initiative of excellence (I-SITE, PIA France) through the Scientific Hub "Metals in Environmental Systems Microbiology (MESMic)."

Credit Statement

Alina Kleindienst: Validation, Formal analysis, Writing – Original Draft, Writing – Review & Editing

Alyssa Azaroff: Conceptualization, Validation, Investigation, Data Curation, Writing – Original Draft, Writing – Review & Editing

Alkuin Koenig: Methodology, Software, Formal Analysis, Writing – Review & Editing, Visualization

Emmanuel Tessier: Investigation, Data Curation, Resources

Claudia Marchan Moreno: Investigation

Zoyne Pedrero Zayas: Supervision

David Amouroux: Conceptualization, Writing - Review and Editing, Supervision, Funding Acquisition

Mathilde Monperrus: Conceptualization, Validation, Investigation, Data Curation, Writing – Original Draft, Writing – Review & Editing, Supervision, Project Administration, Funding Acquisition

4. References

[1] H.M. Amos, D.J. Jacob, D. Kocman, H.M. Horowitz, Y. Zhang, S. Dutkiewicz, M. Horvat, E.S. Corbitt, D.P. Krabbenhoft, E.M. Sunderland, Global Biogeochemical Implications of Mercury Discharges from Rivers and Sediment Burial, Environ. Sci. Technol. 48 (2014) 9514–9522. https://doi.org/10.1021/es502134t.

[2] M. Liu, Q. Zhang, T. Maavara, S. Liu, X. Wang, P.A. Raymond, Rivers as the largest source of mercury to coastal oceans worldwide, Nat. Geosci. 14 (2021) 672–677. https://doi.org/10.1038/s41561-021-00793-2.

[3] R. Chester, The transport of material to the oceans: relative flux magnitudes, in: R. Chester (Ed.), Marine Geochemistry, Springer Netherlands, Dordrecht, 1990: pp. 149–191. https://doi.org/10.1007/978-94-010-9488-7_6.

[4] C.H. Lamborg, C.R. Hammerschmidt, K.L. Bowman, An examination of the role of particles in oceanic mercury cycling, Philos Trans A Math Phys Eng Sci 374 (2016) 20150297. https://doi.org/10.1098/rsta.2015.0297.

[5] A. Azaroff, E. Tessier, J. Deborde, R. Guyoneaud, M. Monperrus, Mercury and methylmercury concentrations, sources and distribution in submarine canyon sediments (Capbreton, SW France): Implications for the net methylmercury production, Science of The Total Environment 673 (2019) 511–521. https://doi.org/10.1016/j.scitotenv.2019.04.111.

[6] G. Compeau, R. Bartha, Methylation and demethylation of mercury under controlled redox, pH and salinity conditions, Applied and Environmental Microbiology 48 (1984) 1203–1207. https://doi.org/10.1128/aem.48.6.1203-1207.1984.

[7] S. Jonsson, A. Andersson, M.B. Nilsson, U. Skyllberg, E. Lundberg, J.K. Schaefer, S. Åkerblom, E. Björn, Terrestrial discharges mediate trophic shifts and enhance methylmercury accumulation in estuarine biota, Science Advances 3 (2017) e1601239. https://doi.org/10.1126/sciadv.1601239.

[8] R. Lavoie, T. Jardine, M. Chumchal, K. Kidd, L. Campbell, Biomagnification of Mercury in Aquatic Food Webs: A Worldwide Meta-Analysis, Environmental Science & Technology 47 (2013). https://doi.org/10.1021/es403103t.

[9] R.A. Lavoie, A. Bouffard, R. Maranger, M. Amyot, Mercury transport and human exposure from global marine fisheries, Sci Rep 8 (2018) 6705. https://doi.org/10.1038/s41598-018-24938-3.

[10] A. Sharif, M. Monperrus, E. Tessier, S. Bouchet, H. Pinaly, P. Rodriguez-Gonzalez, P. Maron, D. Amouroux, Fate of mercury species in the coastal plume of the Adour River estuary (Bay of Biscay, SW France), Science of The Total Environment 496 (2014) 701–713. https://doi.org/10.1016/j.scitotenv.2014.06.116.

[11] B.F. Araujo, S. Osterwalder, N. Szponar, D. Lee, M.V. Petrova, J.B. Pernov, S. Ahmed, L.-E. Heimbürger-Boavida, L. Laffont, R. Teisserenc, N. Tananaev, C. Nordstrom, O. Magand, G. Stupple, H. Skov, A. Steffen, B. Bergquist, K.A. Pfaffhuber, J.L. Thomas, S. Scheper, T. Petäjä, A. Dommergue, J.E. Sonke, Mercury isotope evidence for Arctic summertime re-emission of mercury from the cryosphere, Nat Commun 13 (2022) 4956. https://doi.org/10.1038/s41467-022-32440-8.

[12] Y. Zhang, D.J. Jacob, S. Dutkiewicz, H.M. Amos, M.S. Long, E.M. Sunderland, Biogeochemical drivers of the fate of riverine mercury discharged to the global and Arctic oceans, Global Biogeochemical Cycles 29 (2015) 854–864. https://doi.org/10.1002/2015GB005124.

[13] D. Point, G. Bareille, D. Amouroux, H. Etcheber, O.F.X. Donard, Reactivity, interactions and transport of trace elements, organic carbon and particulate material in a mountain range river system (Adour River, France), J. Environ. Monit. 9 (2007) 157–167. https://doi.org/10.1039/B616312B.

[14] B.F. Araujo, H. Hintelmann, B. Dimock, M.G. Almeida, C.E. Rezende, Concentrations and isotope ratios of mercury in sediments from shelf and continental slope at Campos Basin near Rio de

Janeiro, Brazil, Chemosphere 178 (2017) 42–50. https://doi.org/10.1016/j.chemosphere.2017.03.056.
[15] D. Cossa, R. Buscail, B. Dennielou, O. Radakovitch, P. Puig, A. Khripounoff, B. Boutier, S. Berné, Sources, Transport, and accumulation of Mercury in the northwestern Mediterranean margin sediments during the Industrial Era and influence of turbiditic events, Progress in Oceanography 220 (2024) 103186. https://doi.org/10.1016/j.pocean.2023.103186.
[16] M. Meng, R. Sun, H. Liu, B. Yu, Y. Yin, L. Hu, J. Shi, G. Jiang, An Integrated Model for Input and Migration of Mercury in Chinese Coastal Sediments, Environ. Sci. Technol. 53 (2019) 2460–2471. https://doi.org/10.1021/acs.est.8b06329.
[17] R. Yin, X. Feng, B. Chen, J. Zhang, W. Wang, X. Li, Identifying the Sources and Processes of Mercury in Subtropical Estuarine and Ocean Sediments Using Hg Isotopic Composition, Environ. Sci. Technol. 49 (2015) 1347–1355. https://doi.org/10.1021/es504070y.
[18] M. Ravichandran, Interactions between mercury and dissolved organic matter--a review, Chemosphere 55 (2004) 319–331. https://doi.org/10.1016/j.chemosphere.2003.11.011.
[19] A.T. Schartup, U. Ndu, P.H. Balcom, R.P. Mason, E.M. Sunderland, Contrasting Effects of Marine and Terrestrially Derived Dissolved Organic Matter on Mercury Speciation and Bioavailability in Seawater, Environ. Sci. Technol. 49 (2015) 5965–5972. https://doi.org/10.1021/es506274x.
[20] E. Seelen, V. Liem-Nguyen, U. Wünsch, Z. Baumann, R. Mason, U. Skyllberg, E. Björn, Dissolved organic matter thiol concentrations determine methylmercury bioavailability across the terrestrial-marine aquatic continuum, Nat Commun 14 (2023) 6728. https://doi.org/10.1038/s41467-023-42463-4.
[21] J.M. Benoit, C.C. Gilmour*, R.P. Mason, G.S. Riedel, G.F. Riedel, Behavior of mercury in the Patuxent River estuary, Biogeochemistry 40 (1998) 249–265. https://doi.org/10.1023/A:1005905700864.
[22] A. Campeau, K. Eklöf, A.L. Soerensen, S. Åkerblom, S. Yuan, H. Hintelmann, M. Bieroza, S. Köhler, C. Zdanowicz, Sources of riverine mercury across the Mackenzie River Basin; inferences from a combined HgC isotopes and optical properties approach, Science of The Total Environment 806 (2022) 150808. https://doi.org/10.1016/j.scitotenv.2021.150808.
[23] P.F. Schuster, R.G. Striegl, G.R. Aiken, D.P. Krabbenhoft, J.F. Dewild, K. Butler, B. Kamark, M. Dornblaser, Mercury export from the Yukon River Basin and potential response to a changing climate, Environ Sci Technol 45 (2011) 9262–9267. https://doi.org/10.1021/es202068b.
[24] J.E. Sonke, R. Teisserenc, L.-E. Heimbürger-Boavida, M.V. Petrova, N. Marusczak, T. Le Dantec, A.V. Chupakov, C. Li, C.P. Thackray, E.M. Sunderland, N. Tananaev, O.S. Pokrovsky, Eurasian river spring flood observations support net Arctic Ocean mercury export to the atmosphere and Atlantic Ocean, Proc Natl Acad Sci U S A 115 (2018) E11586–E11594. https://doi.org/10.1073/pnas.1811957115.
[25] T. Stoichev, A.T. de Chanvalon, S. Veloso, J. Deborde, E. Tessier, L. Lanceleur, D. Amouroux, Assessing and predicting the changes for inorganic mercury and methylmercury concentrations in surface waters of a tidal estuary (Adour Estuary, SW France), Marine Pollution Bulletin 186 (2023) 114400. https://doi.org/10.1016/j.marpolbul.2022.114400.
[26] C. Liénart, N. Susperregui, V. Rouaud, J. Cavalheiro, V. David, Y. Del Amo, R. Duran, B. Lauga, M. Monperrus, T. Pigot, S. Bichon, K. Charlier, N. Savoye, Dynamics of particulate organic matter in a coastal system characterized by the occurrence of marine mucilage – A stable isotope study, Journal of Sea Research 116 (2016) 12–22. https://doi.org/10.1016/j.seares.2016.08.001.
[27] M. Jiskra, L.-E. Heimbürger-Boavida, M.-M. Desgranges, M.V. Petrova, A. Dufour, B. Ferreira-Araujo, J. Masbou, J. Chmeleff, M. Thyssen, D. Point, J.E. Sonke, Mercury stable isotopes constrain atmospheric sources to the ocean, Nature 597 (2021) 678–682. https://doi.org/10.1038/s41586-021-03859-8.
[28] M. Liu, W. Xiao, Q. Zhang, S. Yuan, P.A. Raymond, J. Chen, J. Liu, S. Tao, Y. Xu, X. Wang, Substantial accumulation of mercury in the deepest parts of the ocean and implications for the environmental mercury cycle, Proceedings of the National Academy of Sciences 118 (2021) e2102629118. https://doi.org/10.1073/pnas.2102629118.

595 [29] M. Mil-Homens, J. Blum, J. Canário, M. Caetano, A.M. Costa, S.M. Lebreiro, M. Trancoso, T.
596 Richter, H. de Stigter, M. Johnson, V. Branco, R. Cesário, F. Mouro, M. Mateus, W. Boer, Z.
597 Melo, Tracing anthropogenic Hg and Pb input using stable Hg and Pb isotope ratios in
598 sediments of the central Portuguese Margin, Chemical Geology 336 (2013) 62–71.
599 https://doi.org/10.1016/j.chemgeo.2012.02.018.
600 [30] N. Ogrinc, H. Hintelmann, J. Kotnik, M. Horvat, N. Pirrone, Sources of mercury in deep-sea
601 sediments of the Mediterranean Sea as revealed by mercury stable isotopes, Sci Rep 9 (2019)
602 11626. https://doi.org/10.1038/s41598-019-48061-z.
603 [31] B. Bergquist, J. Blum, The Odds and Evens of Mercury Isotopes: Applications of Mass-
604 Dependent and Mass-Independent Isotope Fractionation, Elements 5 (2009) 353–357.
605 https://doi.org/10.2113/gselements.5.6.353.
606 [32] J.D. Blum, L.S. Sherman, M.W. Johnson, Mercury Isotopes in Earth and Environmental Sciences,
607 Annu. Rev. Earth Planet. Sci. 42 (2014) 249–269. https://doi.org/10.1146/annurev-earth-
608 050212-124107.
609 [33] B.A. Bergquist, J.D. Blum, Mass-Dependent and -Independent Fractionation of Hg Isotopes by
610 Photoreduction in Aquatic Systems, Science 318 (2007) 417–420.
611 https://doi.org/10.1126/science.1148050.
612 [34] A.L. Buchachenko, N.N. Lukzen, J. Boiden Pedersen, On the magnetic field and isotope effects in
613 enzymatic phosphorylation, Chemical Physics Letters 434 (2007) 139–143.
614 https://doi.org/10.1016/j.cplett.2006.12.019.
615 [35] E.A. Schauble, Role of nuclear volume in driving equilibrium stable isotope fractionation of
616 mercury, thallium, and other very heavy elements, Geochimica et Cosmochimica Acta 71 (2007)
617 2170–2189. https://doi.org/10.1016/j.gca.2007.02.004.
618 [36] J. Chen, H. Hintelmann, X. Feng, B. Dimock, Unusual fractionation of both odd and even
619 mercury isotopes in precipitation from Peterborough, ON, Canada, Geochimica et
620 Cosmochimica Acta 90 (2012) 33–46. https://doi.org/10.1016/j.gca.2012.05.005.
621 [37] X. Fu, M. Jiskra, X. Yang, N. Marusczak, M. Enrico, J. Chmeleff, L.-E. Heimbürger-Boavida, F.
622 Gheusi, J.E. Sonke, Mass-Independent Fractionation of Even and Odd Mercury Isotopes during
623 Atmospheric Mercury Redox Reactions, Environ. Sci. Technol. 55 (2021) 10164–10174.
624 https://doi.org/10.1021/acs.est.1c02568.
625 [38] M. Enrico, G.L. Roux, N. Marusczak, L.-E. Heimbürger, A. Claustres, X. Fu, R. Sun, J.E. Sonke,
626 Atmospheric Mercury Transfer to Peat Bogs Dominated by Gaseous Elemental Mercury Dry
627 Deposition, Environ. Sci. Technol. 50 (2016) 2405–2412.
628 https://doi.org/10.1021/acs.est.5b06058.
629 [39] B. Boutier, Quintin, Jean-Yves, Rozuel, Emmanuelle, Dominique ,Auger, J. and Bretaudeau-
630 Sanjuan, Retrospective study of metal contamination time trends in the French part of the Bay
631 of Biscay, Environmental Technology 32 (2011) 1807–1815.
632 https://doi.org/10.1080/09593330.2011.557398.
633 [40] T. Stoichev, D. Amouroux, J.C. Wasserman, D. Point, A. De Diego, G. Bareille, O.F.X. Donard,
634 Dynamics of mercury species in surface sediments of a macrotidal estuarine–coastal system
635 (Adour River, Bay of Biscay), Estuarine, Coastal and Shelf Science 59 (2004) 511–521.
636 https://doi.org/10.1016/j.ecss.2003.10.007.
637 [41] S. Veloso, D. Amouroux, L. Lanceleur, C. Cagnon, M. Monperrus, J. Deborde, C. Cravo-Laureau,
638 R. Duran, Keystone microbial taxa organize micropollutant-related modules shaping the
639 microbial community structure in estuarine sediments, Journal of Hazardous Materials 448
640 (2023) 130858. https://doi.org/10.1016/j.jhazmat.2023.130858.
641 [42] A. Borja, D. Amouroux, P. Anschutz, M. Gómez-Gesteira, M.C. Uyarra, L. Valdés, Chapter 5 - The
642 Bay of Biscay, in: C. Sheppard (Ed.), World Seas: An Environmental Evaluation (Second Edition),
643 Academic Press, 2019: pp. 113–152. https://doi.org/10.1016/B978-0-12-805068-2.00006-1.
644 [43] C. Petus, G. Chust, F. Gohin, D. Doxaran, J.-M. Froidefond, Y. Sagarminaga, Estimating turbidity
645 and total suspended matter in the Adour River plume (South Bay of Biscay) using MODIS 250-m

imagery, Continental Shelf Research 30 (2010) 379–392. https://doi.org/10.1016/j.csr.2009.12.007.
[44] T. Stoichev, D. Amouroux, M. Monperrus, D. Point, E. Tessier, G. Bareille, O.F.X. Donard, Mercury in surface waters of a macrotidal urban estuary (River Adour, south-west France), Chemistry and Ecology 22 (2006) 137–148. https://doi.org/10.1080/02757540500526450.
[45] S. Defontaine, D. Sous, D. Morichon, R. Verney, M. Monperrus, Hydrodynamics and SPM transport in an engineered tidal estuary: The Adour river (France), Estuarine, Coastal and Shelf Science 231 (2019) 106445. https://doi.org/10.1016/j.ecss.2019.106445.
[46] M. Gaudin, T. Mulder, P. Cirac, S. Berné, P. Imbert, Past and present sedimentary activity in the Capbreton Canyon, southern Bay of Biscay, Geo-Mar Lett 26 (2006) 331–345. https://doi.org/10.1007/s00367-006-0043-1.
[47] S. Schmidt, H. Howa, A. Diallo, J. Martín, M. Cremer, P. Duros, C. Fontanier, B. Deflandre, E. Metzger, T. Mulder, Recent sediment transport and deposition in the Cap-Ferret Canyon, South-East margin of Bay of Biscay, Deep Sea Research Part II: Topical Studies in Oceanography 104 (2014) 134–144. https://doi.org/10.1016/j.dsr2.2013.06.004.
[48] S. Brocheray, M. Cremer, S. Zaragosi, S. Schmidt, F. Eynaud, L. Rossignol, H. Gillet, 2000 years of frequent turbidite activity in the Capbreton Canyon (Bay of Biscay), Marine Geology 347 (2014) 136–152. https://doi.org/10.1016/j.margeo.2013.11.009.
[49] S. Bouchet, P. Rodriguez-Gonzalez, R. Bridou, M. Monperrus, E. Tessier, P. Anschutz, R. Guyoneaud, D. Amouroux, Investigations into the differential reactivity of endogenous and exogenous mercury species in coastal sediments, Environ Sci Pollut Res 20 (2013) 1292–1301. https://doi.org/10.1007/s11356-012-1068-9.
[50] V. Perrot, V.N. Epov, M.V. Pastukhov, V.I. Grebenshchikova, C. Zouiten, J.E. Sonke, S. Husted, O.F.X. Donard, D. Amouroux, Tracing sources and bioaccumulation of mercury in fish of Lake Baikal--Angara River using Hg isotopic composition, Environ Sci Technol 44 (2010) 8030–8037. https://doi.org/10.1021/es101898e.
[51] P. Rodríguez-González, V.N. Epov, R. Bridou, E. Tessier, R. Guyoneaud, M. Monperrus, D. Amouroux, Species-specific stable isotope fractionation of mercury during Hg(II) methylation by an anaerobic bacteria (Desulfobulbus propionicus) under dark conditions, Environ Sci Technol 43 (2009) 9183–9188. https://doi.org/10.1021/es902206j.
[52] National Institute of Standards & Technology, Report of Investigation Reference Material 8610 Isotopes in UM-Almaden Mono-Elemental Secondary Stndard, National Institute of Standards & Technology, 2017. https://tsapps.nist.gov/srmext/certificates/8610.pdf.
[53] B. Duval, E. Tessier, L. Kortazar, L.A. Fernandez, A. de Diego, D. Amouroux, Dynamics, distribution, and transformations of mercury species from pyrenean high-altitude lakes, Environ Res 216 (2023) 114611. https://doi.org/10.1016/j.envres.2022.114611.
[54] Liénart et al. - 2016 - Dynamics of particulate organic matter in a coasta.pdf, (n.d.).
[55] C. Liénart, N. Savoye, Y. Bozec, E. Breton, P. Conan, V. David, E. Feunteun, K. Grangeré, P. Kerhervé, B. Lebreton, S. Lefebvre, S. L'Helguen, L. Mousseau, P. Raimbault, P. Richard, P. Riera, P.-G. Sauriau, G. Schaal, F. Aubert, S. Aubin, S. Bichon, C. Boinet, L. Bourasseau, M. Bréret, J. Caparros, T. Cariou, K. Charlier, P. Claquin, V. Cornille, A.-M. Corre, L. Costes, O. Crispi, M. Crouvoisier, M. Czamanski, Y. Del Amo, H. Derriennic, F. Dindinaud, M. Durozier, V. Hanquiez, A. Nowaczyk, J. Devesa, S. Ferreira, M. Fornier, F. Garcia, N. Garcia, S. Geslin, E. Grossteffan, A. Gueux, J. Guillaudeau, G. Guillou, O. Joly, N. Lachaussée, M. Lafont, J. Lamoureux, E. Lecuyer, J.-P. Lehodey, D. Lemeille, C. Leroux, E. Macé, E. Maria, P. Pineau, F. Petit, M. Pujo-Pay, P. Rimelin-Maury, E. Sultan, Dynamics of particulate organic matter composition in coastal systems: A spatio-temporal study at multi-systems scale, Progress in Oceanography 156 (2017) 221–239. https://doi.org/10.1016/j.pocean.2017.03.001.
[56] N. Estrade, J. Carignan, J.E. Sonke, O.F.X. Donard, Mercury isotope fractionation during liquid–vapor evaporation experiments, Geochimica et Cosmochimica Acta 73 (2009) 2693–2711. https://doi.org/10.1016/j.gca.2009.01.024.

[57] S. Ghosh, E.A. Schauble, G. Lacrampe Couloume, J.D. Blum, B.A. Bergquist, Estimation of nuclear volume dependent fractionation of mercury isotopes in equilibrium liquid–vapor evaporation experiments, Chemical Geology 336 (2013) 5–12. https://doi.org/10.1016/j.chemgeo.2012.01.008.
[58] J.G. Wiederhold, C.J. Cramer, K. Daniel, I. Infante, B. Bourdon, R. Kretzschmar, Equilibrium Mercury Isotope Fractionation between Dissolved Hg(II) Species and Thiol-Bound Hg, Environ. Sci. Technol. 44 (2010) 4191–4197. https://doi.org/10.1021/es100205t.
[59] W. Zheng, H. Hintelmann, Mercury isotope fractionation during photoreduction in natural water is controlled by its Hg/DOC ratio, Geochimica et Cosmochimica Acta 73 (2009) 6704–6715. https://doi.org/10.1016/j.gca.2009.08.016.
[60] W. Zheng, H. Hintelmann, Isotope Fractionation of Mercury during Its Photochemical Reduction by Low-Molecular-Weight Organic Compounds, J. Phys. Chem. A 114 (2010) 4246–4253. https://doi.org/10.1021/jp9111348.
[61] C. Xiao, H. Jian, L. Chen, C. Liu, H. Gao, C. Zhang, S. Liang, Y. Li, Toxic metal pollution in the Yellow Sea and Bohai Sea, China: distribution, controlling factors and potential risk, Marine Pollution Bulletin 119 (2017) 381–389. https://doi.org/10.1016/j.marpolbul.2017.03.027.
[62] H. Sanei, P.M. Outridge, K. Oguri, G.A. Stern, B. Thamdrup, F. Wenzhöfer, F. Wang, R.N. Glud, High mercury accumulation in deep-ocean hadal sediments, Sci Rep 11 (2021) 10970. https://doi.org/10.1038/s41598-021-90459-1.
[63] W.F. Fitzgerald, C.H. Lamborg, C.R. Hammerschmidt, Marine Biogeochemical Cycling of Mercury, Chem. Rev. 107 (2007) 641–662. https://doi.org/10.1021/cr050353m.
[64] J.D. Demers, J.D. Blum, D.R. Zak, Mercury isotopes in a forested ecosystem: Implications for air-surface exchange dynamics and the global mercury cycle, Global Biogeochemical Cycles 27 (2013) 222–238. https://doi.org/10.1002/gbc.20021.
[65] J.P.G. Barre, S. Queipo-Abad, C. Sola-Larrañaga, G. Deletraz, S. Bérail, E. Tessier, D. Elustondo Valencia, J.M. Santamaría, A. de Diego, D. Amouroux, Comparison of the Isotopic Composition of Hg and Pb in Two Atmospheric Bioaccumulators in a Pyrenean Beech Forest (Iraty Forest, Western Pyrenees, France/Spain), Frontiers in Environmental Chemistry 1 (2020). https://www.frontiersin.org/articles/10.3389/fenvc.2020.582001 (accessed June 2, 2023).
[66] X. Fu, N. Marusczak, X. Wang, F. Gheusi, J.E. Sonke, Isotopic Composition of Gaseous Elemental Mercury in the Free Troposphere of the Pic du Midi Observatory, France, Environ. Sci. Technol. 50 (2016) 5641–5650. https://doi.org/10.1021/acs.est.6b00033.
[67] J.P.G. Barre, G. Deletraz, C. Sola-Larrañaga, J.M. Santamaria, S. Bérail, O.F.X. Donard, D. Amouroux, Multi-element isotopic signature (C, N, Pb, Hg) in epiphytic lichens to discriminate atmospheric contamination as a function of land-use characteristics (Pyrénées-Atlantiques, SW France), Environmental Pollution 243 (2018) 961–971. https://doi.org/10.1016/j.envpol.2018.09.003.
[68] S. Defontaine, D. Sous, D. Morichon, R. Verney, M. Monperrus, Hydrodynamics and SPM transport in an engineered tidal estuary: The Adour river (France), Estuarine, Coastal and Shelf Science 231 (2019) 106445. https://doi.org/10.1016/j.ecss.2019.106445.
[69] S. Yang, P. Li, K. Sun, N. Wei, J. Liu, X. Feng, Mercury isotope compositions in seawater and marine fish revealed the sources and processes of mercury in the food web within differing marine compartments, Water Research 241 (2023) 120150. https://doi.org/10.1016/j.watres.2023.120150.